Algal Research 83 (2024) 103701

Contents lists available at ScienceDirect

Algal Research

journal homepage: www.elsevier.com/locate/algal

The microbiome of bioreactors containing mass-cultivated marine diatoms for industrial carbon capture and utilization

Nerea Johanna Aalto [a,b], Ingeborg Hulda Giæver [a], Gunilla Kristina Eriksen [a], Linn Israelsen [a], Stina Krsmanovic [a], Sebastian Petters [a], Hans C. Bernstein [a,b,*]

[a] Norwegian College of Fisheries Sciences, UiT - The Arctic University of Norway, Tromsø, Norway
[b] The Arctic Centre for Sustainable Energy, UiT - The Arctic University of Norway, Tromsø, Norway

ARTICLE INFO

Keywords:
Algae
Mass cultivation
Phycosphere
Community succession
Porosira glacialis

ABSTRACT

Marine microalgae are a promising innovation platform for carbon capture and utilization (CCU) biotechnologies to mitigate industrial greenhouse gas emissions. However, industrial-scale cultivation of algal mono-cultures is challenging and often unscalable. Non-axenic microalgae in large semi-open photobioreactors lead to the co-cultivation of diverse microbial communities. There is limited knowledge about the "bioreactor ecology" involving microalgae interacting with the microbiome and its subsequent impact on process stability and productivity. In this study, we describe the semi-continuous industrial mass cultivation of the cold-adapted marine diatom, *Porosira glacialis* UiT201, by investigating the prokaryotic and microeukaryotic (phytoplankton and heterotrophic protist) communities. Data were collected in two consecutive time series experiments, representing the initiation and operation of an industrial-scale CCU photobioreactor (300,000 L). The first experiment experienced a culture "crash" of the focal strain after 39 days, while the second culture remained stable and "healthy" for 60 days. The results highlight that this mass cultivation system represents a unique industrial marine microbial ecosystem. The succession of the prokaryotic community was primarily driven by species replacement, indicating turnover due to selective bioreactor conditions and/or biological interactions. Nonetheless, the bioreactor consistently harbors a recurring and abundant core microbiome, suggesting that the closely associated bacterial community is influenced by microalgae-specific properties and can endure a dynamic and variable environment. The observed culture collapse of *P. glacialis* coincided with changes in the core microbiome structure and different environmental growth conditions compared to the stable and "healthy" experiment. These findings imply that cohabiting microbial taxa within industrial microalgae cultivation likely play a critical role in stabilizing the conversion of industrial CO_2 into marine biomass, and changes in community structure serve as an indicator of process stability.

1. Introduction

Growing levels of atmospheric carbon have an impact on biodiversity, human health, the economy, and the global geopolitical landscape. As the world's climate nears new tipping points [1], it is imperative that we not only reduce emissions but also take new steps towards carbon capture and utilization (CCU). Innovative biotechnologies that capitalize on photosynthetic carbon fixation, which naturally controls global carbon cycles, will contribute significantly to the solution [2]. Marine microalgae are specifically promising because they have a much higher carbon fixation capacity than plants. Living microalgae make up just 1–2 % of global biomass, but they account for almost 50 % of the world's primary production [3,4]. The utility of microalgae for CCU is being demonstrated at an industrial installation in (Arctic) northern Norway, that harnesses cold-adapted marine diatoms to capture CO_2 at the source from an operational ferrosilicon smelter plant [5]. This is a prominent example of how innovative algal biotechnology can be deployed for CCU by taking advantage of locally isolated diatom strains adapted to the seasonality and seawater resources available to coastal industry locations. A recent study reported a difference in the photophysiology of the Arctic diatom *Porosira glacialis* UiT201 compared to temperate microalgae that enables strong photosynthetic flexibility in the dynamic light and temperature environment, as is uniquely experienced in coastal, Arctic regions [6].

* Corresponding author at: UiT-The Arctic University of Norway, BFE-fak., Postboks 6050 Langnes, 9037 Tromsø, Norway.
E-mail address: Hans.C.Bernstein@uit.no (H.C. Bernstein).

https://doi.org/10.1016/j.algal.2024.103701
Received 7 November 2023; Received in revised form 12 August 2024; Accepted 7 September 2024
Available online 10 September 2024

Scaling up mass cultivation of microalgae for CCU must, however, overcome several barriers that include managing the microbial populations within large industrial-scale photobioreactors. As axenic mass cultivation of microalgae is technically challenging, large photobioreactors are often populated by multi-domain microbial communities and function as their own unique ecosystems [7,8]. A better understanding of how these communities assemble and behave under stable and unstable – i.e., reactor crash – conditions is needed to scale bioreactors up to volumes capable of effective industrial CO_2 capture. Open airlift column bioreactors are effective for scaled-up industrial operation, land space utilization, and improved CO_2 gas-to-liquid transfer [5]. However, the challenge linked to open-systems is a constant exposure to the environment and thereby capacity of recruiting new microbial taxa to the system [8]. The extent to which a bioreactor recruits microbial taxa from the environment depends on how the inputs (e.g., water, nutrients, innocula) and control volume are exposed to the environment. This presents a unique intersection between bioprocess engineering for CCU and microbial ecology.

Coinhabiting microbial taxa within industrial photobioreactors are not necessarily harmful. In fact, previous studies have demonstrated that the majority of the interspecific interactions between microalgae and bacteria are mutualistic [9–11]. The beneficial associations are based on the exchange of synthesized compounds, enhancing the growth of both partners [12,13]. The invasion of other microbial eukaryotes i.e., phytoplankton and heterotrophic protists (hereafter referred to as "microeukaryotes") instead can cause a rapid culture collapse of the focal strain [8]. Some mass cultivation attempts used euryhaline and high pH tolerate focal strains to prevent the contamination of competitive or predative species [14–16]. However, extreme conditions reduce the number of potential strains and might complicate the operational processes. To uncover the potential and risks associated with the coexisting microbiome, a shift in focus from focal strain-centered investigations to ones that encompass the entire biological component of the production system is necessary [17].

Major knowledge gaps exist in our understanding of how to control or even measure the complex interactions between microalgae and bacteria. Only a few previous studies have measured the microbial diversity of photobioreactors, and none (to our knowledge) have investigated the effects on the stability of CCU-specific operations. In order to address some of these knowledge gaps, mass cultivation of the marine centric diatom *Porosira glacialis* UiT201 in a preindustrial-scale CCU operation was combined with an investigation of the community composition and temporal dynamics of the bioreactor microbiome. This study systematically explores three research questions: (i) Which prokaryotic and microeukaryotic taxa are recurrently observed in mass cultivation alongside the focal diatom strain? (ii) What are the discernible succession patterns within the prokaryotic and microeukaryotic consortia of the bioreactor microbiome, and how are these patterns influenced by the bioreactor's fluctuating environmental conditions? and (iii) In what ways do the outcomes of two sequential time-series experiments, one concluding with a premature culture crash at 39 days and the other achieving sustained culture stability for 60 days, converge or diverge in terms of microbiome structure and bioreactor growth conditions?

2. Materials and methods

2.1. Algae inoculum

The focal strain used to inoculate bioreactors was the centric diatom *Porosira glacialis* (UiT-201). It was originally single-cell isolated from a sediment sample collected in the Barents Sea (N 76° 27.54′, E 033° 03.54′) in 2014 [18]. The monoculture was maintained in a temperature-regulated incubator (Termaks KBP 6151) at 8 °C with a scalar irradiance of 65 μmol m^{-2} s^{-1} and diluted weekly with filtered (0.45 μm) and autoclaved seawater containing inorganic marco- and micronutrients from a plant nutrient mix YaraTera Kristalon Purple (Yara, Norway) and sodium metasilicate pentahydrate ($Na_2SiO_3{\cdot}5H_2O$; Permakem, Norway).

2.2. Photobioreactor operation

Mass cultivation of *P. glacialis* took place in northern Norway (69.22°N; 18.08°E) in two consecutive time series experiments: 19.08–27.09 and 19.10–17.12 in 2021. Hereafter the first time series recording is referred to as "T1-crash" due to unplanned discontinuation of cultivation caused by contamination and collapse of *P. glacialis* culture and the second as "T2-healthy", in which the focal strain was maintained at targeted abundance and growth rates until the end of time series. The cultivation platform is integrated into an industrial ferrosilicon smelting plant, Finnfjord AS, in collaboration with UiT – The Arctic University of Norway. A detailed description of the mass cultivation design and operation is given in Eilertsen et al. [5]. The platform contains four vertical column airlift photobioreactors with volumes of 6 m^3, 6 m^3, 14 m^3, and 300 m^3 [5]. This study deployed the largest 300 m^3 reactor operated with a culture volume of 150 m^3 under semicontinuous conditions. Seawater for cultivation medium was obtained from an adjacent fjord at the depth of 25 m and filtered through a multichannel filtration unit with 0.45 μm as the smallest cartridge pore size and through a UV-sterilization unit (Model: MR3-350PP; Ultraaqua, Denmark). The seawater inflow to the reactor is, however, not sterile, despite the robust filtration system. Compressed air and flue gas from the factory with CO_2 content of 3–7 % were added into the bottom of the reactor using a rotating gas dispersing device [5]. Flue gas was sparged continuously during the cultivation periods except for three dates: 28.10., 08.12., and 14.12.2021. Illumination was provided for the reactors by ambient sunlight plus submerged LED lights. Additional artificial illumination was provided by a collection of 200 × 50 W LED light units placed above the culture surface of the bioreactor. The average light intensity in the 300 m^3 reactor, provided by the collection of sources, was 36 μmol m^{-2} s^{-1}. Inorganic nutrients (nitrite, nitrate, and phosphate) a plant nutrient mix YaraTera Kristalon Purple (Yara, Norway), and $Na_2SiO_3{\cdot}5H_2O$ (Permakem, Norway) were added manually to the culture from the start of T1-crash and following 9-days (19.10.-29.10.2021). Thereafter, the nutrients were automatically added using a dosing pump to ensure continuous addition of nutrients. On average, 1231 g 24 h^{-1} of Kristalon Purple and 1321 g 24 h^{-1} of $Na_2SiO_3{\cdot}5H_2O$ were dosed as liquid solutions into the bioreactor.

2.3. Inoculation of the 300 m^3 photobioreactor

Prior to each time series experiment, the inoculation volume of *P. glacialis* was increased in two smaller (6 m^3 and 14 m^3) bioreactors. The 300 m^3 bioreactor was pre-filled with ~45,000 L of filtered seawater before the inoculum was introduced. Thereafter, the volume was increased for the next two days until a volume of 150 m^3 was reached, as this was the maximum operation capacity for the light delivery system. Semicontinuous operation was maintained by continuously adding filtered seawater for five days a week (Monday – Friday morning) with a mean inflow of 2100 L h^{-1}. The culture surplus was extracted from overflow (150 m^3) and algae was harvested.

2.4. Sample collection and growth condition monitoring

Daily measurements were obtained during scheduled work shifts (Monday-Friday) from the 300 m^3 bioreactor for: temperature (C°; Endress-Hauser sensor iTHERMA ModuLine TM131 w) and dissolved oxygen (DO mg L^{-1}; WTWMulti 360 m with CellOx 325 sensor, Xylem Anlaytics, Welheim, Germany) from subsurface at ~1 m depth. Liquid samples for cell counts were collected daily and for analysis of inorganic nutrients every second day. Samples were collected twice weekly (Monday and Friday) for genomic DNA isolation and dissolved organic

carbon (DOC mg L^{-1}). These samples were also collected from the 300 m^3 bioreactor pre-filled with filtered intake water (hereafter referred to as "SW bioreactor"), from inoculum (samples from 6 m^3 and 14 m^3 were combined), and once or twice from intake water used to semi-continuously dilute the reactor.

2.5. Sample processing and analyses

Concentration of inorganic nutrients of nitrite-nitrate ($NO_2^- + NO_3^-$), phosphate (PO_4^{3-}), and silicate ($Si(OH)_4$) were analyzed immediately after filtering sample through a GF/C microfiber filter (Whatman). A nutrient specific Spectroquant kit (Merck Millipore, US) was used, and the concentration was determined spectrophotometrically using a 96-well plate with a microplate reader (FilterMax F5, Molecular Devices, CA), in which the absorbance was measured at 540 nm. DOC samples were filtered through 0.2 μm cellulose syringe filters (Corning®) into acid-washed and pre-combusted 60 mL glass vials and stored in the dark at +4 °C for 12 months before acidification with 250 μl of 2 N HCl to determine the concentration with a TOC-VPH analyzer (Shimadzu, Japan). Modified Utermöhl method was used to obtain an estimation of *P. glacialis* cell density. Cells from two separate transects were counted from a 4-well dish with an inverted light microscope (Zeiss PrimoVert) after 2 h of settling (Nunc, Thermo Fisher Scientific, US). Depending on the culture density, up to 1 L of sample was filtered through each ($n = 5$ per sampling day) 0.22 μm Sterivex polyethersulfone membrane filter unit (Millipore) to obtain biomass for DNA extraction and following amplicon sequencing of 16S and 18S small subunit ribosomal RNA (SSU rRNA) genes. The filters were immediately stored at −80 °C for 3 months before DNA extraction took place at the UiT – The Arctic University of Norway.

2.6. Microbiome – DNA extraction and Illumina amplicon sequencing

DNeasy Power Water Kit (Qiagen, Carlsbad, CA) was used for the purification of genomic DNA. DNA was extracted from the collected biomass following the manufacturer's protocol and stored at −80 °C until PCR. DNA quality and quantity were assessed by the NanoDrop™ Spectrophotometer and Qubit fluorometer (Invitrogen TM). Bacterial communities were identified following the Earth Microbiome Project (EMP) [19] 16S Standard Illumina library preparation protocol, using the forward-barcoded 515f (5′-3′ GTGYCAGCMGCCGCGGTAA) [20] and 806r (5′-3′ GGACTACNVGGGTWTCTAAT) [21] primers targeting the V4 region of 16S SSU rRNA. Targeted gene sequencing of microeukaryotes was determined following the EMP 18S Illumina Amplicon Protocol using the universal Euk_1391f (5′-3′ AATGATACGGCGACCACCGAGATCTACAC) and the barcoded EukBr (5′-3′ TGATCCTTCTGCAGGTTCACCTAC) primers targeting the V9 region of the 18S SSU rRNA [22,23]. The PCR products were confirmed by gel electrophoresis in 1 % agarose gels and visualized with GelRed® staining. Sequencing was performed on an Illumina MiSeq instrument (Illumina, San Diego, CA) at the Environmental Sample Preparation and Sequencing Facility at Argonne National Laboratory (Lemont, IL, USA).

2.7. Microbiome–Bioinformatic pipeline

Forward and reverse Illumina reads were imported into QIIME2 and thereafter demultiplexed using the complementary barcode file, for each sequencing run, respectively. These steps were executed using the EMP paired-end flag. DADA2 V2021.0 algorithm within QIIME2 was used for denoising and merging the reads [24]. During the denoising steps of the DADA2 package, the reads were pooled, filtered and chimera-checked. Additionally, the replicated reads were discarded. After removing the chimeric sequences and singletons, the reads of the 16S runs and 18S runs were merged, respectively. The DADA2 statistic on sequence reads is provided in Supplementary Data S1. Subsequently, the DADA2 package was used for inferring and filtering amplicon sequence variants (ASVs). Taxonomy was assigned by aligning these ASV sequences against the SILVA V138.1 database, using a 16S and 18S rRNA self-trained classifier [25,26]. Classifiers were trained using RESCRIPt [27]. Although the 16S and 18S based taxonomic classification within SILVA V138.1 database is a standardized approach, it has limitations regarding classification and taxonomic resolution. It is noted that manual correction of taxonomic annotation was beyond the scope of this study. Nevertheless, order *Enterobacterales* was manually changed to order *Alteromonadales* as the main classified families obtained within *Enterobacterales* in our 16S dataset were *Colwelliaceae*, *Alteromonadaceae* and *Pseudoalteromonadaea* that are known to be members of *Alteromonadales* [28]. The phylogenetic rooted tree, generated with QIIME2 using MAFFT algorithm, was used for downstream diversity analysis.

2.8. Microbiome–Diversity analysis

All downstream analyses were completed using R [29]. The microbiome time-series data was analyzed using the "microeco" package (v16.0) [30] unless another package is specifically mentioned. Prior to community analysis, all reads that belonged to mitochondria, chloroplast, and kingdom *Eukaryota* or were unassigned (no assigned kingdom) were removed from the 16S dataset. Filtering from the 18S dataset removed ASVs assigned to the kingdoms of *Bacteria* and *Archaea* and phyla of *Vertebrata*, *Arthropoda*, *Nematozoa*, *Annelida*, *Cnidaria*, *Mollusca*, *Tunicate*, *Phragmoplastophyta*, and *Basidiomycota*, as well as unassigned reads. Both datasets, 16S and 18S, contained a high number of ASVs with a low number of reads. For example, 2074 ASVs found just in 300 m^3 bioreactor comprised only 0.6 % of the total reads within the 16S dataset. As we are only considering taxa with higher abundance, an abundance-filter was used to remove rare and possibly ambiguous ASVs from the datasets. The filter-threshold included only ASVs, which mean relative abundance within the complete 16S and 18S datasets was >0.01 %, respectively. As a result of this, the number of ASVs decreased from 7736 to 430 and from 1577 to 58 within the 16S and 18S datasets, respectively. After these filtration steps, the final library size comprised 5908–18,328 and 2924–417,990 reads in 16S and 18S datasets, respectively. Counts of unique ASVs per sample were used to measure richness and Shannon's diversity index was used to combine both richness and evenness – i.e., alpha-diversity [31]. The `multcomp´R package was used to perform a post hoc multiple comparison test with Tukey's HSD [32] on the alpha-diversity of different sample types between and within T1-crash and T2-healthy using generalized linear models with Poisson distribution. Potential core prokaryotic taxa associated with the focal strain from inoculum to the end of time series were identified applying an occurrence filter with a 75 % presence threshold separately on T1-crash and T2-healthy 16S datasets.

The compositional differences in prokaryotic and microeukaryotic communities – i.e., beta diversity was measured with an unweighted Jaccard distance metric to emphasize presence/absence of community members. Three sample days, both from the beginning and the end of the 300 m^3 bioreactor time series, were included to infer how the bioreactor microbiome composition in the start and end differs and how they relate to the communities in inoculum, intake water, and SW bioreactor (pre-filled 300 m^3 reactor with filtrated seawater). The community differences were visualized in Principal Coordinate Analysis (PCoA) and the pairwise permutational multivariate analysis of variance (PERMANOVA) was performed to test the (dis)similarity associated with each sample type and chosen time series fraction within and between T1-crash and T2-healthy. Beta diversity was also measured via Jaccard distances between T1-crash and T2-healthy bioreactor time series samples, respectively. The Jaccard distances were partitioned to account for the contributions of "nestedness" (species loss) and "turnover" (species gain) towards the measure of total dissimilarity – i.e., $\beta_{Jac} = \beta_{Jne} + \beta_{Jtu}$ [33,34]. This was obtained using the R package `betapart´ [35]. The associated changes within total beta diversity, turnover, and nestedness, respectively, by sampling day were tested using "adonis" function

(PERMANOVA) with 999 permutations from the R package `vegan´ [36]. Taxonomic recruitment of prokaryotes across time series experiments was estimated by calculating the fraction of ASVs that were unobserved at any previous cultivation days [34]. This metric was adapted from the data analysis of a previous study investigating community succession and is available at https://github.com/pnnl/brislawn-2018-founders-species.

2.9. Microbiome–Clustering around temporal patterns

The K-medoids clustering method was depolyed following the previously described approach applied to microbiome time series data [37,38]. It was used to investigate shifts in microbiome structure by examining community members that share similar succession patterns across the crash and healthy time series. Prior to clustering, the ASV counts were preprocessed through normalization steps including variance stabilizing transformation (R package `DESeq2) [39], detrending (R package `pracma) [40], and scaling via z-transformation to convert values on a z-score scale to ensure intercomparability between ASVs. As the K-medoids is a distance-based clustering method, pairwise Euclidean distances were calculated before each ASV was partitioned into K clusters according to similarity criterion using the R package `cluster [41]. The clustering efficacy – a balance between number of clusters and data overfitting – was assessed via the Calinski-Harabasz index (Supplementary Fig. S1) [42,43].

2.10. Growth conditions of 300 m^3 bioreactor – Statistics

The Mann-Whitney *U* test (also known as the Wilcoxon rank sum test) was performed to reveal differences in bioreactor physical and biogeochemical conditions between T1-crash and T2-healthy. The potential association between the measured bioreactor conditions and their relationship with identified temporal patterns (cluster medoids) was obtained using Spearman's rank correlation analysis. Non-parametric analyses were conducted as half of the included factors indicated non-normal distribution based on the Shapiro-Wilk normality test (Supplementary Table S1).

2.11. Data repository and reproducible analyses

The unprocessed genetic sequencing data for both SSU rRNA 16S and 18S gene amplicons is available in ENA repository under project PRJEB66331. All data, including ASV, taxonomy and relative abundance tables, and bioreactor measurements used for analysis and graphing, along with the R markdown script, are available on the Open Science Framework (osf.io) as part of this project: https://osf.io/k2egy/.

3. Results

3.1. The bioreactor's microbiome

Open mass cultivation of marine diatoms within the industrial CCU setting resulted in a complex microbiome that accompanied growth of the target strain *P. glacialis*. The prokaryotic and microeukaryotic community members were diverse and relatively dynamic during both crashed and healthy cultivation periods. This was observed across two time series experiments with lengths of 39 (crashed) and 60 days (healthy), respectively. The first time series – T1-crash – ended with the loss of dominating abundance of the focal strain, *P. glacialis*, as determined by a decrease in growth, and microscopy observations revealed severe increases of dead and lysed cells. During the second time series from a mass cultivation run – T2-healthy – *P. glacialis* kept its growth and abundance until the operation was ended and biomass was harvested after 60 days. Despite the major differences in conditions and outcomes, the observed richness and diversity, especially for the prokaryotic component of the microbiome, across both time series experiments shared major similarities (Fig. 1 and Supplementary Fig. S2). The total number of prokaryotic ASVs in T1-crash was 339 and in T2-healthy 368, and the corresponding microeukaryotic richness was 47 and 56 ASVs, respectively. Prokaryotic richness and diversity (Shannon) measured in the 300 m^3 bioreactor did not differ between the T1-crash and T2-healthy (Tukey's HSD results given in Supplementary Table S2 and S3), as in total 291 and 256 unique ASVs were observed across time (Fig. 1a,b), and the Shannon diversity index ranged from 1.7 to 3.2 in T1-crash and 1.6 to 3.2 in T2-healthy (Supplementary Fig. S2). However, only 54–128 ASVs in T1-crash and 49–113 in T2-healthy were present in each sample day, which corresponds to the richness measured within each inoculum, but not within the SW bioreactor (pre-filled 300 m^3 reactor with filtrated seawater) or intake water samples, which comprised a higher number of ASVs (Fig. 1a, b). A clear decrease in Shannon diversity was observed in the middle of T1-crash and T2-healthy. As a somewhat similar pattern was observed in richness, especially in T2-healthy, the change was only partially driven by evenness. The microeukaryotic portion of the bioreactor microbiome (measured via 18S rRNA gene amplicons) showed mainly a contrasting result as compared to the prokaryotic community (Fig. 1c, d). The SW reactor and intake water samples comprised a smaller or corresponding number of unique ASVs than the inoculum and per day 300 m^3 bioreactor samples. Also, the mean number of observed ASVs but not Shannon diversity in the bioreactor across time was significantly different between T1-crash and T2-healthy (Tukey's HSD, $p < 0.001$; Supplementary Table S4 and S5). In both time series, the richness and changes that occurred over time were somewhat similar until day 32. Thereafter, the number of observed ASVs stayed constant in T2-healthy, whereas in T1-crash a strong decrease was observed towards the end (Fig. 1c, d). This pattern was not inferred from the Shannon diversity index, which instead revealed similar diversity, especially at the end of both time series experiments (Supplementary Fig. S2).

3.2. Mass cultivation has an abundant core microbiome

Nearly the same number of ASVs and taxonomic assignments within prokaryotes were found when ASVs were filtered on occurrence (i.e., presence) at a threshold of 75 % among the inoculum and 300 m^3 bioreactor samples. These were 27 and 21 in T1-crash and 25 and 22 in T2-healthy, respectively, that were present throughout the mass cultivation runs. The core ASVs accounted for 20–50 % of the unique ASVs observed each sample day in the bioreactor of both time series runs. Fourteen of the core ASVs, categorized into nine different bacterial orders, were discovered in the bioreactor and inoculum of the two time series periods. Between 44 % and 91 % of the prokaryotic community's daily relative abundance in T1-crash and, correspondingly, between 33 % and 91 % in T2-healthy, were the taxa that the core ASVs were classified into (core and other ASV(s), henceforth referred to as core taxa) (Fig. 2a, b). Supplementary Table S6 contains a list of all the core ASVs together with the corresponding taxonomic assignments.

3.3. The reactor's prokaryotic community structure was distinct between crash versus healthy production

When the 16S ASVs were allocated to the taxonomic level order, the prokaryotic community in both time series studies exhibited a dominance of three groups (Fig. 2a, b). Specifically, in the T1-crash, the community was dominated by taxa classified within the order *Rhodobacterales* (22 %–75 % of the relative abundance) until cultivation day-11, comprising mainly ASVs assigned to the genus *Planktotalea* (Fig. 2a). In the T2-healthy, *Rhodobacterales* became the most abundant class at the end of the time series after cultivation day-46 (28 %–54 % of relative abundance) and was dominated by ASVs not assigned to a lower taxonomic level (Fig. 2b). Taxa indicative of the order *Flavobacteriales* were predominant, notably ASVs assigned to genera NS9 marine group and *Winogradskyella*, for the first half of the T2-healthy time series with the

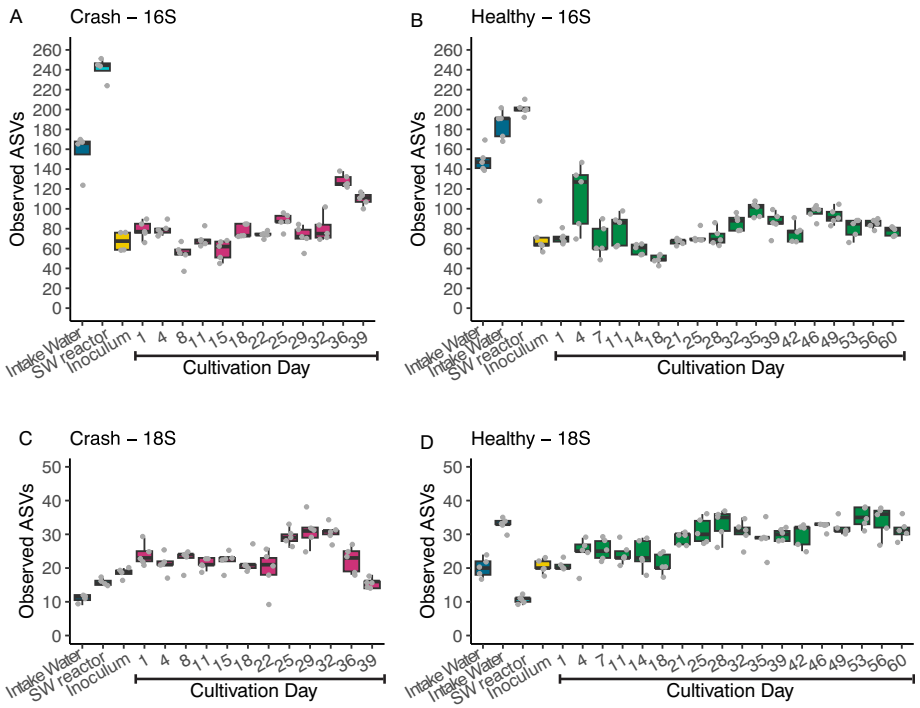

Fig. 1. Alpha diversity measured as the observed number of unique ASVs in each sample type and across bioreactor time series cultivations. Prokaryotic richness (16S) in time series experiment (A) crash and (B) healthy. Microeukaryotic richnes (18S) in time series experiment (C) crash and (D) healthy. The values of biological replicates ($n = 4$ or $n = 5$) are shown over boxplots. Note the different y-axis range between 16S and 18S datasets.

exception of cultivation day-14, while in T1-crash the predominance of the same genera was shorter and limited in the middle of the time series (Fig. 2a, b). The third predominant prokaryotic order was different between the time series experiments as taxa classified within order *Chitinophagales*, mainly ASVs assigned to the family *Saprospiraceae*, became the most abundant in the end of T1-crash (25 %–64 % of relative abundance) (Fig. 2a). Whereas in the T2-healthy, taxa classified as *Opitutales*, comprised almost solely by genus indicative of *Lentimonas*, had a high relative abundance in most of the cultivation days and was the most abundant on cultivation day-14 (49 % of the relative abundance) and in the middle of the second half of the time series (Fig. 2b).

3.4. The bioreactor's microeukaryotic community structure was similar until the culture collapse in T1-crash

The focal strain, *P. glacialis*, is currently classified within class *Mediophyceae* [44], although this classification was not given by the SILVA v138 database as 19 different ASVs indicative to class *Mediophyceae* were assigned under the same annotation (*Mediophyceae*) down to genus level. Among these ASVs, ASV *032943128192fa7f0a17b2d2991a72f4* comprised a 2–3 magnitude higher number of reads compared to the other ASVs. It is therefore considered that most of the relative abundance within class *Mediophyceae* is composed by the focal strain, *P. glacialis*, in the 18S microeukaryotic communities.

The community structure of microeukaryotes at the taxonomic level class was similar between T1-crash and T2-healthy samples until a rapid turn from *P. glacialis* dominance to predominance of ASVs classified within the class *Bacillariophyceae* after cultivation day 29 (59 %–89 % of relative abundance) in T1-crash (Fig. 2c, d). It is notable that members of *Bacillariophyceae* were present from the start in both time series with similar abundances until strong occupation took place in T1-crash, whereas in T2-healthy the relative abundance stayed constant until the end of the experiment. This contamination was caused by small pennate diatoms, as confirmed by preliminary microscopic detection (Supplementary Fig. S3). The most abundant ASV within *Bacillariophyceae* was *f030aa085cd7c8b4bb6538425a95161c*. ASVs assigned to the class *Bacillariophyceae* were also present in the community in the SW bioreactor and intake water samples in the T1-crash, but to a lower degree in the T2-healthy run, where taxa representative of the class *Chrysophyceae* were prevalent, particularly in the intake water. However, *Chrysophyceae* did not show increasing occupation across time in the T2-healthy microbiome (Fig. 2c, d).

3.5. Beta diversity–Microbiome community composition between sample types and across time

The community composition of prokaryotes and microeukaryotes changed from inoculation to the end-point in both time series experiments as inferred from pairwise PERMANOVA comparison of the three first (start) and last (end) sample days (T1-crash: 16S, $R^2 = 0.50$ and $p < 0.01$ & 18S, $R^2 = 0.61$ and $p < 0.01$; T2-healthy: 16S, $R^2 = 0.61$, $p < 0.01$ & 18S, $R^2 = 0.63$, $p < 0.01$). The communities within start- and end-time fractions were significantly dissimilar to those obtained in corresponding inoculum, intake water, and SW bioreactor samples, and these sample types were also dissimilar in relation to each other (Supplementary Table S7 and S8). The Jaccard dissimilarity distances within 16S and 18S datasets, respectively, were visualized by ordination with PCoA, which showed that 39.7 % and 44.0 % of the total variation among all included prokaryotic and microeukaryotic samples, respectively, were explained by the two first principal coordinate axes (Fig. 3). Closer inspection of the ordination results indicated that in both time series experiments, the community composition in the early time series was more similar with the parallel inoculum community, except for microeukaryotes in T1-crash, than in the end, as the communities exhibited strong differentiation across time (Fig. 3). The communities within SW bioreactor and intake water were clearly distinct from those in inoculum and 300 m^3 bioreactor samples but also from each other, although the 300 m^3 bioreactor was pre-filled with intake water (Fig. 3).

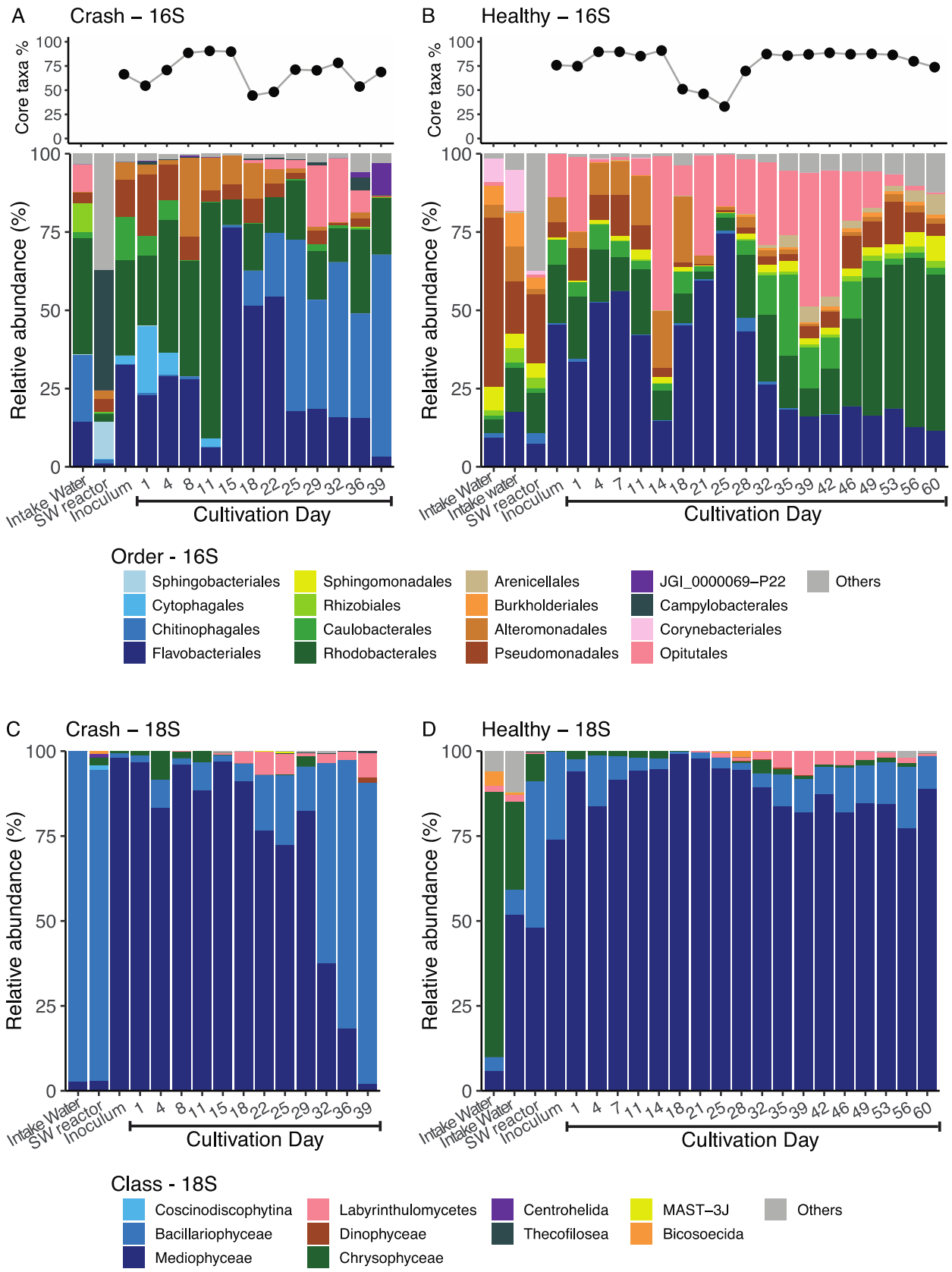

Fig. 2. Comparison of community structure in each sample type and across bioreactor time series cultivations. The change in relative abundance of core taxa (core ASVs and other ASVs classified within the same taxonomic assignment) from inoculum to cultivation end and the taxonomic composition of the most abundant prokaryotes classified within taxonomic level order in (A) crash and (B) healthy time series. Taxonomic composition of the most abundant microeukaryotes classified within taxonomic level class in (C) crash and (D) healthy time series.

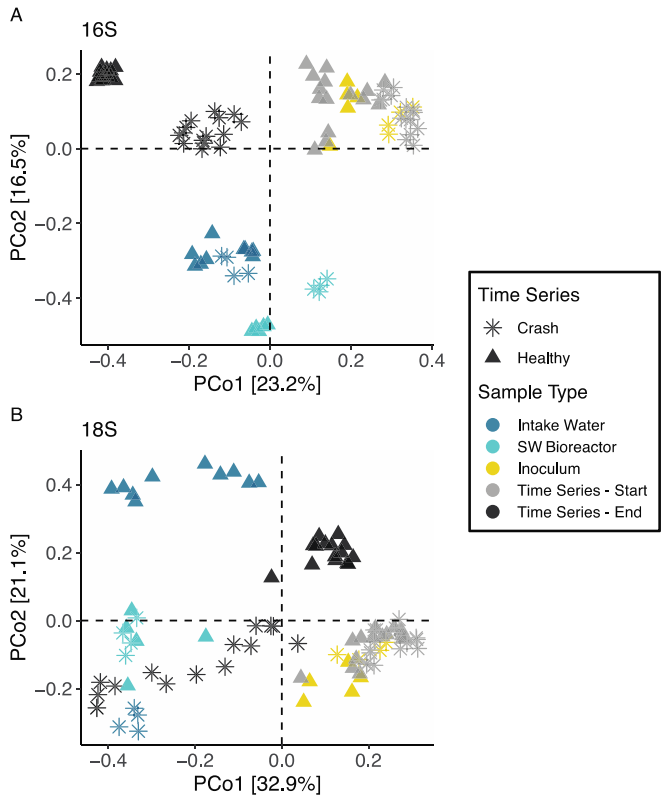

Fig. 3. Beta diversity in prokaryotic and microeukaryotic community composition between sample types and bioreactor time series start- and end-time fractions measured with unweighted Jaccard distances and visualized via Principal coordinate analysis. Dissimilarity within (A) prokaryotic and (B) microeukaryotic communities. Time series start-time fraction comprises cultivation days 1, 4, and 8 in crash and 1, 4, and 7 in healthy experiment. The corresponding end-time fractions are 32, 36, and 39 for crash and 53, 56, and 60 for healthy time series.

3.6. Beta diversity–Contribution of species-loss and replacement to the bioreactor's community succession patterns

Temporal variation in the community composition of the bacterial fraction of the microbiome was driven to a greater degree by turnover (species replacement) than nestedness (species loss) in both time series (Fig. 4a, b). This inference was obtained by analysis that disentangles the additive contributions of these two antithetic processes to the total beta diversity (as measured by the Jaccard distance) between all-time points across T1-crash and T2-healthy, respectively [33]. The variance attributed to the sampling day was much lower from nestedness than from turnover and total Jaccard in both time series, as these explained over 84 % and 78 % of the observed temporal variation associated with the time points, respectively, in both time series runs (Fig. 4 and Supplementary Table S9). Strong turnover is also indicated by the observed prokaryotic richness, which stayed rather constant across T1-crash and T2-healthy, as under nestedness some level of decrease would be expected through temproal species loss (Fig. 1).

The bioreactor is exposed to several sources of new taxa that were not continuously monitored in this study, including the input sea water and factory particulate matter from the air. Therefore, the recruitment of prokaryotes was inferred from a metric that indicates the fraction of new taxa introduced to the system at each time point in the time series experiments (Fig. 4c). The results revealed that the system is exposed to the detectable seed bank of available community members very quickly. The introduction of previously unobserved ASVs clearly decreased after the 11–14 days of cultivation, and <8 % and <5 % of the ASVs were new in the rest of the cultivation days in T1-crash and T2-healthy, respectively (Fig. 4c). Although both of the time series experiments indicated a similar pattern, the T1-crash recruited new taxa faster than T2-healthy towards the end of the time series.

3.7. Temporal succession patterns and cooccurring taxa in distinct bioreactor growth environments

The physical and chemical environment in the large 300 m^3 photobioreactor, as well as cell density of *P. glacialis*, were different between mass cultivation runs. This was established using the Mann-Whitney *U* test that showed statistically significant differences between *P. glacialis* cell number and raw fluorescence, concentration of inorganic nutrients, DOC, and bioreactor temperature – i.e., most of the monitored factors except pH level (Supplementary Table S10). The measured values of these factors were higher in T2-healthy compared to the T1-crash, apart from DOC concentration and bioreactor temperature, which were lower (Fig. 5 and Supplementary Fig. S4).

The potential association of community members to the variable bioreactor environment that prevailed across the time series experiments was evidenced through correlation with temporal patterns. A K-medoid clustering algorithm was used to reduce the temporal complexity within the bioreactor microbiome by identifying the major temporal patterns and revealing the related community members within each time series (T1-crash and T2-healthy) and dataset (16S and 18S). The ASVs within both time series and datasets were divided into three clusters based on assessment of the Calinski-Harabasz index, which was used as a quality metric (Supplementary Fig. S1) [43]. The succession patterns among prokaryotes, as represented by a cluster-specific medoid taxon, revealed that part of the community members from both time series datasets (cluster 2 in T1-crash and T2-healthy) exhibited similar temporal dynamics with an increase in abundance in the middle of the time series (Fig. 6a, b). The medoid of these clusters indicated a significant positive relationship to one of the two factors measuring *P. glacialis* cell density. Yet, the association to the other growth condition factors was not consistent (Fig. 6c, d). Also, most of the prokaryotic taxa within cluster 2 (T1-crash and T2-healthy) belonged to the same highly abundant orders: *Flavobacteriales*, *Rhodobacterales*, *Opitutales* and *Alteromonadales* (Fig. 6e, f). The K-medoid clustering also identified a high number of prokaryotes in the T1-crash (cluster 1 and 3) that first decreased and thereafter increased in their abundance towards the culture crash of *P. glacialis* (Fig. 6a). Especially in cluster 1, the temporal pattern of medoid showed a strong inverse relationship with *P. glacialis* cell density and DOC concentration and indicated an intensive proliferation of ASVs classified within *Rhodobacterales* and *Chitinophagales* in the last two sample days, as these orders comprised the major taxonomic groups within this cluster (Fig. 6c, d).

The cluster medoids identified within the 18S microeukaryotic community revealed a strong fluctuation in relative abundances and weak correlation to bioreactor conditions across time in both time series (Fig. 7a-d). ASVs classified within class *Mediophyceae* and *Bacillariophyceae* were the main groups driving distinct temporal patterns in T1-crash and T2-healthy. In both time series experiments, the class *Bacillariophyceae* belonged to a cluster in which the medoid exhibited a strong decrease in relative abundance in the middle of time series (Fig. 7e, f).

4. Discussion

This study was designed to measure and compare the microbial community succession patterns of an industrial-scale CCU photobioreactor during both successful and crashed operations. While contamination control is important, it is not usually feasible to operate large-scale, open-airlift photobioreactors as axenic cultures of microalgae. Hence, industrial-scale production of microalgal biomass in open systems is also mass cultivation of the associated microbial community members. This is not necessarily a hindrance to the goals of algal CCU

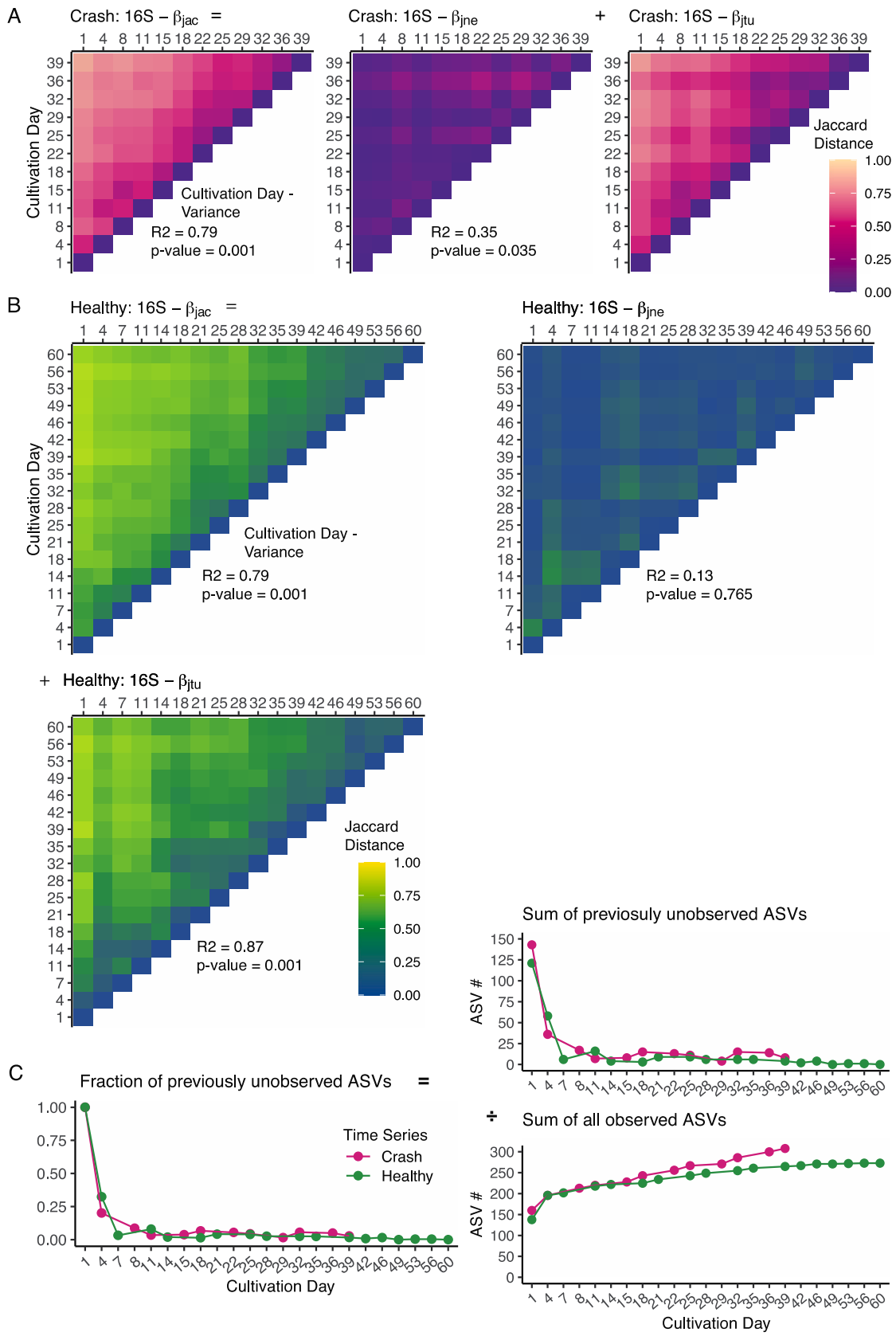

Fig. 4. Changes in prokaryotic communities across time. Unweighted Jaccard distance measured between cultivation days in (A) crash and (B) healthy time series experiments. The total Jaccard distance (β_{jac}) is partitioned by contributions from nestedness (β_{jne}; species loss) and turnover (β_{jtu}; species replacement), i.e., $\beta_{jac} = \beta_{jne} + \beta_{jtu}$. Lighter color represents cultivation days with high dissimilarity. Variance and corresponding significance associated with cultivation day are shown for each process. Introduction of new prokaryotic ASVs over time in crash and healthy time series experiments (C). The fraction of previously unobserved ASVs equals the number of ASVs that were not observed in any of the previous cultivation days and the sum of the total number of ASVs observed at the corresponding time point.

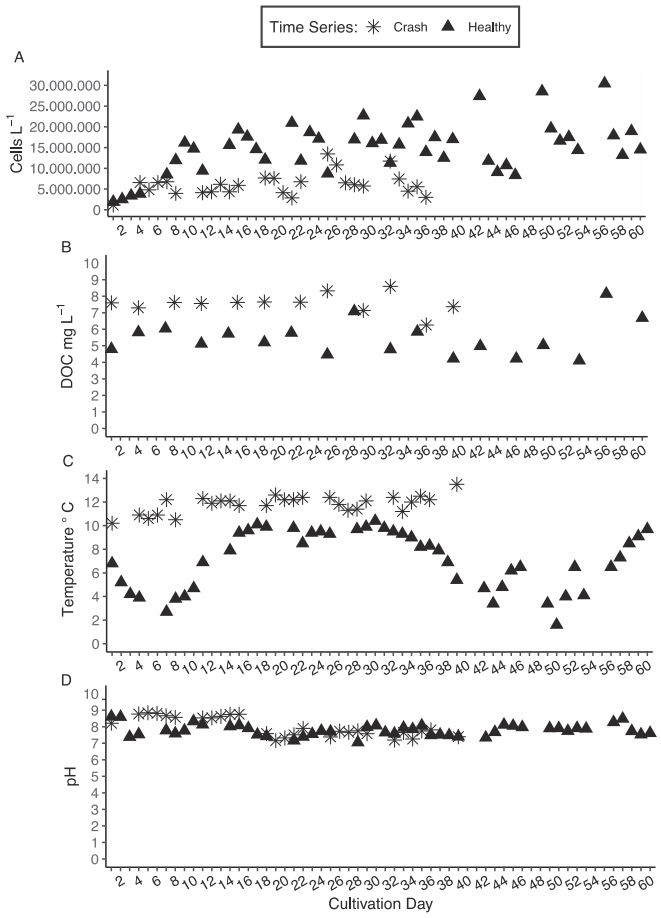

Fig. 5. Variation in bioreactor environment across time in crash and healthy cultivation. Daily or twice a week measurements of (A) *P. glacialis* cell density, (B) DOC concentration, (C) bioreactor temperature, and (D) pH level. Note that the time series crash ended after cultivation day-39.

where pure cultures are not required for success if the bioreactor environment can effectively select for a stable microbial community that promotes growth and abundant proliferation of a focal strain capable of converting CO_2-enriched flue gas into biomass and bioproducts**.** This study highlights an example of how a unique core microbiome, associated with cold-water marine environments, stabilizes within a photobioreactor used for mass cultivation of diatoms and how these types of microbiomes represent an important signature and possibly a controlling variable associated with successful operation.

4.1. *CCU bioreactors are unique industrial marine microbial ecosystems*

This study characterized a diverse microbial ecosystem within an industrial-scale photobioreactor that was distinct from seawater inflow and inoculum (Figs. 2 and 3). This is despite the fact that the operation has been designed to promote growth of large marine diatoms – i.e., *P. glacialis*. The microbial community structure is also sensitive to unique temporal succession patterns that serve as signatures of success or crash. New taxa are recruited to the system via inputs from the semicontinuous inflow of seawater from the adjacent coastal bay [45] and likely the air-water exchanges within the industrial environment. The majority of taxonomic recruitment was observed within the prokaryotic portion of the microbiome, but observations were also made with respect to microeukaryotic taxa. However, the reactor microbiome's recruitment of new prokaryotic taxa stabilizes very quickly (Fig. 4c). Although the bioreactor might be exposed to a larger number of taxa, e.g., ASVs removed by the 0.01 % abundance threshold or ASVs not detected, these taxa are not taking hold in the community. Changes in community structure were observed on the time scale of days, in a similar fashion to previous observations from temperate and coastal cold-water microbial ecosystems [38,46]. It is expected that the diverse community comprises members with different ecological properties, which potentially have a strong impact on the function of the production system in relation to CCU [17]. In addition, most of the major bacteria groups *Flavobacteriales*, *Rhodobacterales*, and orders within *Gammaproteobacteria* found in the 300 m^3 bioreactor have frequently been reported to associate with diatom-driven phytoplankton blooms in natural ecosystems or in diatom monoculture experiments (Fig. 2a, b) [11,31,47,48].

Bacteria that are commonly associated with marine diatoms are known to utilize different alga-derived organic substrates – i.e., DOC that is released across different bloom or growth stages or generated through temporal substrate degradation [46,49]. These dynamic processes at least partially underpin the successional blooming patterns of the prokaryotic groups that were identified in this study and other investigations [38,47]. The orders *Opitutales* (*Verrumicrobiota*) and *Chitinophagales*, which also belonged to the most abundant community ASVs from the current study are not considered either uncommon or specific to our production system as they have also been documented in environmental and experimental studies. Members within *Opitutales* are likely part of a free-living community thriving in eutrophic environments such as wastewater related microalgae cultivations, with a capacity to degrade complex polysaccharides [50]. Members within the *Saprospiraceae* family (*Chitinophagales*) have been reported to interact with diatoms [51].

4.2. *Importance of a strong core microbiome in mass cultivation*

The relatively long and consecutively repeated temporal coverage on microbial community composition provided us an excellent opportunity to infer reoccurring community succession processes. The bioreactor harbors a prominent core microbiome, although the taxonomic composition underwent effective replacement of prokaryotes (strong turnover) between time points (Fig. 4). We found that the core ASVs comprised a high portion of the total number of unique ASVs observed on each sample day in both time series. Many prokaryotic taxa that are introduced by intake water and the pre-filled bioreactor at the beginning are replaced after a while as they do not integrate into the core community, as evidenced by the strong contribution of turnover towards total community dissimilarity. Consequently, the bioreactor functions as a selective environment because of the very different physical and biogeochemical conditions that these taxa suddenly encounter in comparison to the coastal environment, such as low pH and elevated levels of light, nutrients, and DOC, or because of the core taxa's competition and antagonistic relationships, which inhibit the growth of the other taxa. It is also expected that *P. glacialis* imposes a selective force that shapes the core microbiome as partially evinced by the observed changes in the prokaryotic community when small pennate contaminates supplanted the *P. glacialis* focal strain. The relative strength of diatom-driven selection compared to the physical bioreactor environment remains unclear, although it is understood that the closely associated community is structured in a microalgae-specific manner and can persist through environmental variation [12,52,53]. The high similarity in the core microbiome between the two cultivation experiments indicates a certain level of specificity with the production system as it is designed for mass cultivation of *P. glacialis*. It is noted that at least part of the taxa introduced to the bioreactor by intake water influx may reside in the system below detection or were excluded from the analysis along with the applied abundance filter (0.01 %). The core taxa (including core and other ASVs classified within the same taxonomic assignment) accounted for an average of 69 % and 77 % of the relative abundance within bioreactor samples taken from T1-crash and T2-healthy, respectively (Fig. 2a, b). Nevertheless, on the majority of sample days, the high

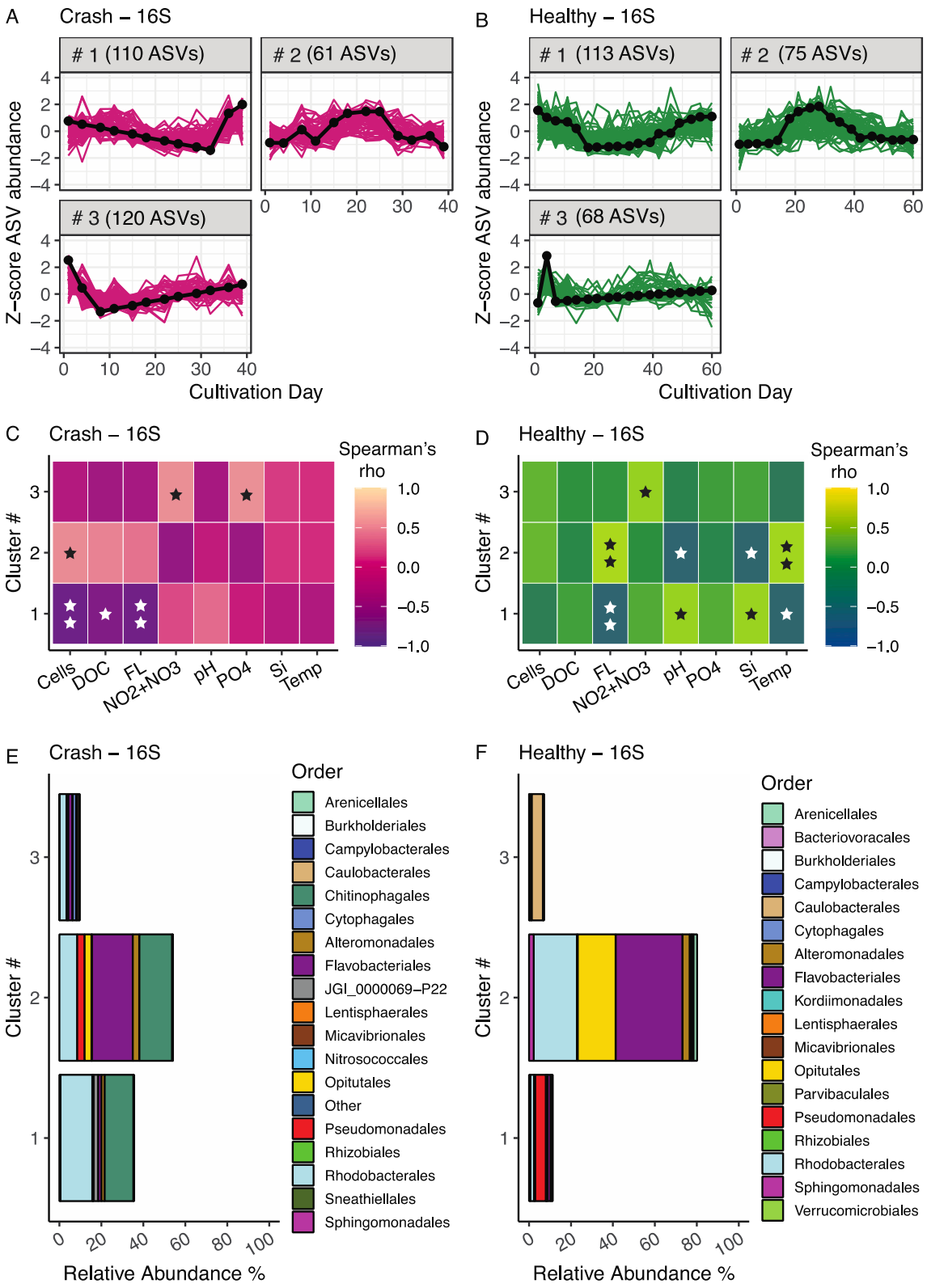

Fig. 6. The major temporal succession patterns within prokaryotic communities as assessed via K-medoid clustering analysis with z-transformation and detrending of 16S ASVs. Temproal dynamics of prokaryotic taxa and identified number of ASVs in bioreactor (A) crash and (B) healthy time series experiments. The black line indicates cluster-specific medoid taxon, a representative for the cluster's temporal pattern. ASV-specific z-score is a y-axis, and a value 0 denotes the mean abundance. Heatmap of Spearman's correlation between temporal dynamics of cluster-specific medoid taxon (z-scores) and measured bioreactor factors in time series (C) crash and (D) healthy. The color indicates Spearmna's rank correlation coefficient (rho), and the significance is denoted with ★ (★, $p \leq 0.05$; ★★, $p \leq 0.01$; ★★★, $p \leq 0.001$). Cells, *P. glacialis* cell density L^{-1}; DOC, DOC mg L^{-1}; FL, raw fluorescence as a proxy for increase/decrease of *P. glacialis* cell density; NO2-NO3, $NO_2^- + NO_3^-$ μM; pH, pH level; PO4, PO_4^{3-} μM; Si, $Si(OH)_4$ μM, Temp, bioreactor temperature °C. The most common prokaryotic taxa at the taxonomic level order within each cluster and their mean relative abundance in a whole community in time series (E) crash and (F) healthy.

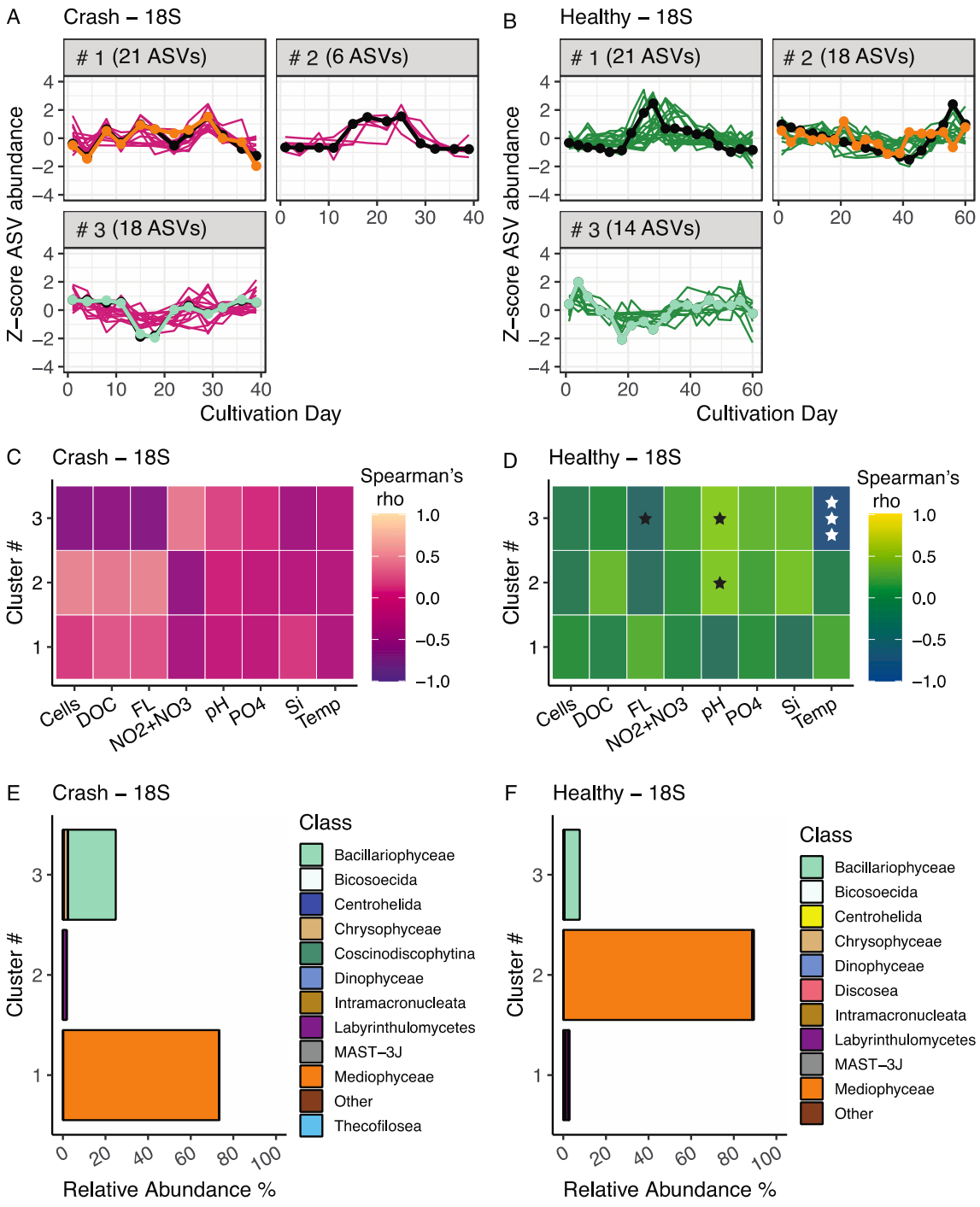

Fig. 7. The major temporal succession patterns within microeukaryotic communities as assessed via K-medoid clustering analysis with z-transformation and detrending of 16S ASVs. Temproal dynamics of prokaryotic taxa and identified number of ASVs in bioreactor (A) crash and (B) healthy cultivation experiments. The black line indicates cluster specific medoid taxon, a representative for the cluster's temporal pattern. ASV-specific z-score is a y-axis, and a value 0 denotes the mean abundance. The orange line specifies temporal dynamics of the most abundant ASVs classified as *Mediophyceae*, representing an expected focal strain, and the light green line specifies the most abundant ASVs classified as *Bacillariophyceae*, representing a potential pennate contaminant. Heatmap of Spearman's correlation between temporal dynamics of cluster-specific medoid taxon (z-scores) and measured bioreactor factors in time series (C) crash and (D) healthy. The color indicates Spearmna's rank correlation coefficient (rho), and the significance is denoted with ★(★, $p \leq 0.05$; ★★, $p \leq 0.01$; ★★★, $p \leq 0.001$). Cells, *P. glacialis* cell density L^{-1}; DOC, DOC mg L^{-1}; FL, raw fluorescence as a proxy for increase/decrease of *P. glacialis* cell density; NO2-NO3, $NO_2^- + NO_3^-$ μM; pH, pH level; PO4, PO_4^{3-} μM; Si, Si $(OH)_4$ μM, Temp, bioreactor temperature °C. The most common microeukaryotic taxa at the taxonomic level class within each cluster and their mean relative abundance in a whole community in time series (E) crash and (F) healthy. (For interpretation of the references to color in this figure legend, the reader is referred to the web version of this article.)

abundance was accounted for by a small number of core taxa, whose predominance fluctuated and was only permanent for a short while. Consequently, the temporal change in the prokaryotic community structure was significantly influenced by a small subset of core taxa. The effects of strong temporal variations in community structure and the interactions of the (core) microbiome on the productivity, stability, and/or controllability of the production system are not well understood. Increasing complexity, or the number of interactions within cooccurring relationships, might positively affect stability and, in turn, have an impact on the growth and biomass concentration of the focal strain. [54]. On the other hand, a previous study on the microbiome of marine sponges inferred that a dense core microbiome with few abundant taxa had a stronger positive impact on community-level stability than more diverse assemblies of sparsely abundant taxa. [55].

4.3. *P. glacialis is a promising candidate for mass cultivation*

Despite the relatively diversified coinhabiting microbiome, *P. glacialis* grows robustly in the mass cultivation system from inoculation through semicontinuous operation of the 300 m^3 photobioreactor. While this work is the first to look at the whole community of the bioreactor, mass cultivation of *P. glacialis* for CCU has been successfully demonstrated in industrial-scale trials for several years before [5]. Reactor crash events are rare, and conversion of industrial CO_2 to *P. glacialis* biomass is typically successful at scale, regardless of cooccurring microeukaryotes identified in this study. This relatively novel marine diatom is a viable agent for large-scale algal CCU and production of high-value biomass [18].

4.4. *Biological factors associated with reactor crash*

Even with a well-controlled inoculation and a robust start during mass cultivation, the reactor can occasionally crash. One of the main obstacles when expanding the size of a bioreactor or switching from a closed to an open cultivation system is the high input water volume delivered into the reactor in production systems with (semi)continuous operation, which makes them susceptible to contamination. This is a well-recognized challenge for open cultivation systems, even though bioreactor crash events are rarely documented in peer-reviewed scientific literature. The research reports on biomass production collapse or culture crash often attribute it to contaminants exhibiting predatory behavior or resource competition [8,15,56]. In the present study, the culture collapse in T1-crash was presumably not caused by predation but rather competition or antagonist interactions from another marine diatom or a member from the prokaryotic community. Our study design does not allow for a conclusive mechanistic understanding of the factors that lead to the culture crash; however, our findings suggest two taxa that showed temporal blooming patterns in relation to the observed crash. The *Saprospiraceae* family (order *Chitinophagales*) was the only highly prevalent member of the core community in T1-crash but not in T2-healthy. As algicidal activity has been connected to filamentous members of *Saprospiraceae* [51,57], the presence of an antagonistic community member against *P. glacalis* should be confirmed in further investigations. We also observed a strongly increasing abundance of pennate diatoms within class *Bacillariophyceae* towards the end of T1-crash, supported by intake water inflow (Fig. 2c), that might have caused competition over resources. Although the cause behind the culture crash remains highly tentative, our findings provide a premise for targeted experiments to uncover taxa with functions that inhibit algal production in this specific industrial system.

4.5. *Variable environments and blooming patterns within the bioreactor*

The large-scale mass cultivation system is also unique in relation to the prevailing environment created in the bioreactor and therefore difficult to replicate. This is primarily a result of seasonal variations in the coastal environment and constant production optimization. Although the measured growth conditions varied and were distinct between the time series experiments, the K-medoids clustering did not reveal a clear correlation between the temporal abundance patterns of microeukaryotes and bioreactor factors. Instead, the impact on the prokaryotic community structure might have been stronger (Fig. 6). For example, the direct impact of lower and more variable temperature in T2-healthy than in T1-crash on the growth of focal strain was probably minor, as *P. glacialis* is shown to obtain a strong growth across the temperature range of 2–12 °C [18]. The growth rate of marine bacteria is known to have a pronounced positive relationship within the similar temperature range [58]. Also, an elevated temperature was reported to increase the abundance of microalgae-associated bacteria and simultaneous carbon assimilation when natural seawater was studied in experimental conditions [59]. Moreover, major differences were observed in the cell density of *P. glacialis* and the biogeochemical environment. While the cell density of *P. glacialis* was clearly lower across T1-crash than T2-healthy, the measured DOC concentration revealed the opposite (Fig. 5). The dataset does not provide a clear insight on why the DOC level was almost constantly 2.1 mg L^{-1} higher in T1-crash than in T2-healthy or how it potentially governed the cooccurring microbial community. DOC excretion can reflect the physiological state of microalgae as a response to stress, or it can be triggered by biological interactions [60–62]. The lower cell density in this case does not directly relate to decreased growth (before culture crash), which in turn could indicate stress because the dilution rate was higher in T1-crash than T2-healthy. However, the concentration of inorganic nutrients, especially silicate in the first half of the time series, was clearly lower in T1-crash than in T2-healthy and therefore might have impacted the cellular response of *P. glacialis* (Supplementary Fig. S4).

4.6. *Core microbiome–An important milestone for further research*

This study uncovered the core microbiome associated with mass cultivation of microalgae for CCU and elucidates the role of recurring prokaryotic taxa associated with the open, large-scale industrial photobioreactor designed to biomass production of the cold-water diatom *P. glacialis*. The findings of this study show that a stable and recurring core microbiome can significantly influence the productivity and stability of industrial-scale open photobioreactors. The core microbiome, comprising key prokaryotic taxa within orders assigned to *Flavobacteriales*, *Rhodobacterales*, and *Opitutales*, shows resilience and adaptability within the dynamic environment of the bioreactor, suggesting relationships that support the growth of the focal diatom strain, *P. glacialis*. However, the specific functional roles of these core microbial members remain unexplored. Understanding these roles will unlock insights into optimizing bioreactor conditions and enhancing biomass yield and CO_2 removal from industrial flue gas. Applying targeted experiments using isolation and laboratory coculturing of the members from the core community with *P. glacialis* alongside metagenomic and -transcriptomic methods is essential [12,63]. Also, continuing monitoring the microbiome succession and community profiles over variable production environments and processes enables unraveling the occasional detrimental contaminants in this unique production system. The knowledge will support future research focusing on microbiome engineering to selectively promote beneficial microbial interactions while suppressing antagonistic species that lead to culture crashes [64]. By manipulating the microbial community structure through targeted interventions, it may be possible to achieve higher efficiency and stability in CCU processes, thereby advancing the scalability and economic feasibility of these industrial scale marine diatom cultivation systems.

5. Conclusion

This work shows how basic concepts of marine microbial ecology can be used to gain a better understanding of, and perhaps even control over,

a promising industrial biotechnology for CCU. Nevertheless, it is difficult to determine the mechanistic influence of the microbiome on biomass production in large industrial-scale photobioreactors since they are difficult and expensive to modify and operate with high replication for experimental purposes only. Each cultivation run of the large vertical photobioreactor is distinct in terms of the cooccurring microbiome community dynamics and maintained growth conditions throughout the *P. glacialis* production process because of its location within a highly seasonal coastal factory setting. However, the reactor is home to a relatively diverse microbial ecosystem that transforms into a core microbiome via turnover of taxa introduced by the inoculum as well as continuous seawater intake and air exposure to factory particles. Alterations in the core microbiome may influence or result from declining and or stablized growth of *P. glacialis*. Consequently, the unique signature of the reactor's microbiome is indicative of stable carbon capture and utilization operations, playing a pivotal role in the efficient conversion of industrial CO_2 into marine biomass.

Funding

This work was supported by the project AlgScaleUp, funded by the Research Councile of Norway as part of the Green Platform (NFR project number: 328654) and ABSORB – Arctic Carbon Storage from Biomes, which is a strategic funding inniative from UiT – The Arctic University of Norway (https://site.uit.no/absorb/). The bioinformatics computations were performed on resources provided bySigma2 - the National Infrastructure for High-Performance Computing and Data Storage in Norway.

CRediT authorship contribution statement

Nerea Johanna Aalto: Writing – review & editing, Writing – original draft, Methodology, Investigation, Formal analysis, Data curation, Conceptualization. **Ingeborg Hulda Giæver:** Methodology, Investigation, Data curation. **Gunilla Kristina Eriksen:** Project administration, Methodology, Investigation, Formal analysis. **Linn Israelsen:** Methodology, Investigation, Formal analysis. **Stina Krsmanovic:** Supervision, Project administration, Methodology, Investigation, Formal analysis, Data curation. **Sebastian Petters:** Visualization, Software, Methodology, Formal analysis, Data curation. **Hans C. Bernstein:** Writing – review & editing, Writing – original draft, Visualization, Validation, Supervision, Software, Resources, Project administration, Methodology, Investigation, Funding acquisition, Formal analysis, Conceptualization.

Declaration of competing interest

The authors declare that they have no known competing financial interests or personal relationships that could have appeared to influence the work reported in this paper.

Data availability

I have shared the link to my data/code in my manuscript

Acknowledgements

This project was made possible through tight collaboration and technical support from Finnfjord AS, with specific acknowledgements to Hans Christian Eilertsen, Jo Strømholt, John-Steinar Bergum and Geir-Henning Wintervoll.

Appendix A. Supplementary data

Supplementary data to this article can be found online at https://doi.org/10.1016/j.algal.2024.103701.

References

[1] Masson-Delmotte, V., et al., IPCC special report: global warming of 1.5° C. Summary for Policymakers. https://www.ipcc.ch/sr15/chapter/spm/, 2018.
[2] H. Schweitzer, et al., Innovating carbon-capture biotechnologies through ecosystem-inspired solutions, One Earth 4 (1) (2021) 49–59.
[3] C.B. Field, et al., Primary production of the biosphere: integrating terrestrial and oceanic components, science 281 (5374) (1998) 237–240.
[4] M.J. Behrenfeld, et al., Biospheric primary production during an ENSO transition, Science 291 (5513) (2001) 2594–2597.
[5] H.C. Eilertsen, et al., Mass cultivation of microalgae: I. Experiences with vertical column airlift photobioreactors, diatoms and CO2 sequestration, Appl. Sci. 12 (6) (2022) 3082.
[6] J.B. Svenning, et al., Lipidome plasticity enables unusual photosynthetic flexibility in Arctic vs, Temperate Diatoms. Marine Drugs 22 (2) (2024) 67.
[7] S.P. Fulbright, et al., Bacterial community changes in an industrial algae production system, Algal Res. 31 (2018) 147–156.
[8] F.K. Davies, et al., Microbiota Associated with the Large-Scale Outdoor Cultivation of the Cyanobacterium Synechococcus Sp, PCC 7002. vol. 58, Algal Research, 2021, p. 1023 82.
[9] S.A. Amin, M.S. Parker, E.V. Armbrust, Interactions between diatoms and Bacteria, Microbiol. Mol. Biol. Rev. 76 (3) (2012) 667–684.
[10] B.P. Durham, et al., Cryptic carbon and sulfur cycling between surface ocean plankton, Proc. Natl. Acad. Sci. 112 (2) (2015) 453–457.
[11] A. Buchan, et al., Master recyclers: features and functions of bacteria associated with phytoplankton blooms, Nat. Rev. Microbiol. 12 (10) (2014) 686–698.
[12] J.-B. Raina, et al., Chemotaxis shapes the microscale organization of the ocean's microbiome, Nature 605 (7908) (2022) 132–138.
[13] S.A. Amin, et al., Interaction and signalling between a cosmopolitan phytoplankton and associated bacteria, Nature 522 (7554) (2015) 98–101.
[14] S.L. Meseck, Controlling the growth of a cyanobacterial contaminant, Synechoccus sp., in a culture of Tetraselmis chui (PLY429) by varying pH: implications for outdoor aquaculture production, Aquaculture 273 (4) (2007) 566–572.
[15] N. von Alvensleben, et al., Salinity tolerance of Picochlorum atomus and the use of salinity for contamination control by the freshwater cyanobacterium Pseudanabaena limnetica, PLoS One 8 (5) (2013) e63569.
[16] M. Haines, et al., Pilot-scale outdoor trial of a cyanobacterial consortium at pH 11 in a photobioreactor at high latitude, Bioresour. Technol. 354 (2022) 127173.
[17] J. Lian, et al., The effect of the algal microbiome on industrial production of microalgae, Microb. Biotechnol. 11 (5) (2018) 806–818.
[18] J.B. Svenning, et al., Temperature dependent growth rate, lipid content and fatty acid composition of the marine cold-water diatom Porosira glacialis, Algal Res. 37 (2019) 11–16.
[19] L.R. Thompson, et al., A communal catalogue reveals Earth's multiscale microbial diversity, Nature 551 (7681) (2017) 457–463.
[20] A.E. Parada, D.M. Needham, J.A. Fuhrman, Every base matters: assessing small subunit rRNA primers for marine microbiomes with mock communities, time series and global field samples, Environ. Microbiol. 18 (5) (2016) 1403–1414.
[21] A. Apprill, et al., Minor revision to V4 region SSU rRNA 806R gene primer greatly increases detection of SAR11 bacterioplankton, Aquat. Microb. Ecol. 75 (2) (2015) 129–137.
[22] L.A. Amaral-Zettler, et al., A method for studying protistan diversity using massively parallel sequencing of V9 hypervariable regions of small-subunit ribosomal RNA genes, PLoS One 4 (7) (2009) e6372.
[23] T. Stoeck, et al., Multiple marker parallel tag environmental DNA sequencing reveals a highly complex eukaryotic community in marine anoxic water, Mol. Ecol. 19 (2010) 21–31.
[24] B.J. Callahan, et al., DADA2: high-resolution sample inference from Illumina amplicon data, Nat. Methods 13 (7) (2016) 581–583.
[25] C. Quast, et al., The SILVA ribosomal RNA gene database project: improved data processing and web-based tools, Nucleic Acids Res. 41 (D1) (2012) D590–D596.
[26] P. Yilmaz, et al., The SILVA and "all-species living tree project (LTP)" taxonomic frameworks, Nucleic Acids Res. 42 (D1) (2014) D643–D648.
[27] M.S. Robeson, et al., RESCRIPt: Reproducible sequence taxonomy reference database management, PLoS Comput. Biol. 17 (11) (2021) e1009581.
[28] A.C. Parte, et al., List of prokaryotic names with standing in nomenclature (LPSN) moves to the DSMZ, International Journal of Systematic and Evolutionary Microbiology 70 (11) (2020) 5607.
[29] R Core Team, *R: A language and environment for statistical computing, R Foundation for Statistical Computing.* 2021.
[30] C. Liu, et al., Microeco: an R package for data mining in microbial community ecology, FEMS Microbiol. Ecol. 97 (2) (2021) fiaa255.
[31] N.J. Aalto, et al., Diversity and selection of surface marine microbiomes in the Atlantic-influenced Arctic, Front. Microbiol. 13 (2022) 892634.
[32] T. Hothorn, F. Bretz, P. Westfall, Simultaneous inference in general parametric models, Biometrical Journal: Journal of Mathematical Methods in Biosciences 50 (3) (2008) 346–363.
[33] A. Baselga, The relationship between species replacement, dissimilarity derived from nestedness, and nestedness, Glob. Ecol. Biogeogr. 21 (12) (2012) 1223–1232.
[34] C.J. Brislawn, et al., Forfeiting the priority effect: turnover defines biofilm community succession, ISME J. 13 (7) (2019) 1865–1877.
[35] A. Baselga, C.D.L. Orme, Betapart: an R package for the study of beta diversity, Methods Ecol. Evol. 3 (5) (2012) 808–812.
[36] Oksanen, J., et al., *Community ecology package.* R package version, 2013. 2(0).
[37] A.R. Coenen, et al., A primer for microbiome time-series analysis, Front. Genet. 11 (2020) 310.

[38] N.J. Aalto, et al., Microbial community dynamics during a harmful Chrysochromulina leadbeateri bloom in northern Norway, Appl. Environ. Microbiol. 89 (1) (2023) p. e01895–22.
[39] M.I. Love, W. Huber, S. Anders, Moderated estimation of fold change and dispersion for RNA-seq data with DESeq2, Genome Biol. 15 (12) (2014) 1–21.
[40] Borchers, H.W. and M.H.W. Borchers, *Package 'pracma'*. accessed on, 2022. 4.
[41] M. Maechler, et al., Package 'Cluster', Dosegljivo na, 2013.
[42] E. Lord, et al., Using the stability of objects to determine the number of clusters in datasets, Inf. Sci. 393 (2017) 29–46.
[43] T. Caliński, J. Harabasz, A dendrite method for cluster analysis, Communications in Statistics-theory and Methods 3 (1) (1974) 1–27.
[44] M.D. Guiry, G.M. Guiry, AlgaeBase., World-Wide Electronic Publication, National University of Ireland, Galway, 2022. http://www.algaebase.org.
[45] N.J. Aalto, et al., *Drivers of atmosphere-ocean CO2 flux in northern Norwegian fjords.* Frontiers in marine, Science (2021) 841.
[46] H. Teeling, et al., Substrate-controlled succession of marine bacterioplankton populations induced by a phytoplankton bloom, Science 336 (6081) (2012) 608–611.
[47] H. Teeling, et al., Recurring patterns in bacterioplankton dynamics during coastal spring algae blooms, elife 5 (2016) e11888.
[48] H. Schäfer, et al., Genetic diversity of 'satellite'bacteria present in cultures of marine diatoms, FEMS Microbiol. Ecol. 42 (1) (2002) 25–35.
[49] F. Eigemann, et al., Phytoplankton producer species and transformation of released compounds over time define bacterial communities following phytoplankton dissolved organic matter pulses, Appl. Environ. Microbiol. 89 (7) (2023) p. e00539–23.
[50] L.H. Orellana, et al., Verrucomicrobiota are specialist consumers of sulfated methyl pentoses during diatom blooms, ISME J. 16 (3) (2022) 630–641.
[51] G. Furusawa, et al., Algicidal activity and gliding motility of Saprospira sp. SS98-5, Can. J. Microbiol. 49 (2) (2003) 92–100.
[52] J. Mönnich, et al., Niche-based assembly of bacterial consortia on the diatom Thalassiosira rotula is stable and reproducible, ISME J. 14 (6) (2020) 1614–1625.
[53] S.L. Jackrel, et al., Host specificity of microbiome assembly and its fitness effects in phytoplankton, ISME J. 15 (3) (2021) 774–788.
[54] M.B. Paddock, J.D. Fernández-Bayo, J.S. VanderGheynst, The effect of the microalgae-bacteria microbiome on wastewater treatment and biomass production, Appl. Microbiol. Biotechnol. 104 (2) (2020) 893–905.
[55] J.R. Björk, et al., The dynamic core microbiome: structure, dynamics and stability, BioRxiv 10 (2017) 137885.
[56] Y. Wang, et al., Identification of harmful protozoa in outdoor cultivation of Chlorella and the use of ultrasonication to control contamination, Algal Res. 31 (2018) 298–310.
[57] McIlroy, S.J. and P.H. Nielsen, *The family saprospiraceae.* The Prokaryotes: Other Major Lineages of Bacteria and The Archaea.[4th ed.], 2014: p. 863–889.
[58] P.A. White, et al., The effect of temperature and algal biomass on bacterial production and specific growth rate in freshwater and marine habitats, Microb. Ecol. 21 (1991) 99–118.
[59] N. Arandia-Gorostidi, et al., Warming the phycosphere: differential effect of temperature on the use of diatom-derived carbon by two copiotrophic bacterial taxa, Environ. Microbiol. 22 (4) (2020) 1381–1396.
[60] M. Mühlenbruch, et al., Mini-review: phytoplankton-derived polysaccharides in the marine environment and their interactions with heterotrophic bacteria, Environ. Microbiol. 20 (8) (2018) 2671–2685.
[61] A. Gärdes, et al., Effects of Marinobacter adhaerens HP15 on polymer exudation by Thalassiosira weissflogii at different N: P ratios, Mar. Ecol. Prog. Ser. 461 (2012) 1–14.
[62] C.J. Hulatt, D.N. Thomas, Dissolved organic matter (DOM) in microalgal photobioreactors: a potential loss in solar energy conversion? Bioresour. Technol. 101 (22) (2010) 8690–8697.
[63] J. Lian, et al., Different co-occurring bacteria enhance or decrease the growth of the microalga Nannochloropsis sp. CCAP211/78, Microb. Biotechnol. 14 (3) (2021) 1159–1170.
[64] H. Hu, et al., Guided by the principles of microbiome engineering: accomplishments and perspectives for environmental use, Mlife 1 (4) (2022) 382–398.